Check for updates

Stability of [10–12]cycloparaphenylene complexes with pristine fullerenes $C_{76,78,84}$ and endohedral metallofullerenes $M_3N@C_{78,80}$†

Markus Freiberger,‡[a] Olga A. Stasyuk, [ID] ‡[b] M. Eugenia Pérez-Ojeda, [ID] [a]
Luis A. Echegoyen, [ID] [c,d] Miquel Solà [ID] *[b] and Thomas Drewello [ID] *[a]

[n]Cycloparaphenylenes ([n]CPPs) are strained macrocycles, comprising only sp^2-hybridized carbon atoms. In recent years, [n]CPPs have become of great research interest in the field of supramolecular chemistry since their special structure enables the formation of novel host–guest complexes. In this work, we investigate the gas-phase chemistry of noncovalent complexes of [10−12]CPP with the pristine fullerenes $C_{76/78/84}$ and the endohedral metallofullerenes (EMFs) $Sc_3N@D_{3h}$-C_{78}, $Sc_3N@D_{5h}$-C_{80} and $M_3N@I_h$-C_{80} (M = Sc, Y, Lu, Gd). The [1 : 1] complexes with [10−12]CPP are detected as radical cations. The stability and charge distributions of these complexes are studied using energy-resolved collision-induced dissociation (ER-CID). Our results assess the size complementarity, the influence of fullerene symmetry and size as well as the role of the metal size inside the EMF on the binding affinity and complex stability. Two main trends in complex stability have been found: First, [10−12]CPP form more stable complexes with EMFs than with pristine fullerenes and second, all complexes of EMFs with the C_{80} skeleton show similar stability despite the different metal clusters encapsulated. Another major finding is the fact that [11]CPP is generally the most suitable host for fullerenes with a $C_{76/78/80/84}$ skeleton. Considering the charge distributions, we observe the existence of two different fragmentation channels for complexes with EMFs where the radical cation is either located at the CPP or at the EMF: (1) $[n]CPP^{+•}$ + EMF and (2) $[n]CPP$ + $EMF^{+•}$. This behavior allows a clear distinction of the cage isomers ($[11]CPP \supset Sc_3N@I_h$-$C_{80})^{+•}$ and $([11]CPP \supset Sc_3N@D_{5h}$-$C_{80})^{+•}$ in the MS^2 experiment. The experimental results are accompanied by density functional theory (DFT) calculations of ionization potentials (IPs) and fragmentation energies. The computational results fully confirm the measured order of complex stabilities and explain the prevalence of EMF or CPP signals in the spectra by the trend in ionization potentials.

Introduction

The groundbreaking discovery of multi-walled carbon nanotubes[1] and fullerene peapods[2] paved the way for three decades of intensive research regarding the supramolecular chemistry of carbon networks with curved π-systems. Particularly, the possibility to alter the unique electronic properties of carbon nanotubes by encapsulating guest molecules, such as the

endohedral metallofullerenes (EMFs) $Gd@C_{82}$,[3] $La_2@C_{80}$,[4,5] $Dy@C_{82}$,[6] $Ce@C_{82}$,[7] *etc.* attracted considerable attention. Cycloparaphenylenes (CPPs) represent the shortest sidewall segment of armchair carbon nanotubes.[8] Since their first synthesis in 2008,[9] CPPs and their derivatives have become intensively studied model systems in the field of supramolecular chemistry. An important aspect regarding the complexation of CPPs with fullerenes is the size and the shape complementarity of both entities.[10,11] The so far most studied CPP-fullerene host–guest system is certainly the $[10]CPP \supset C_{60}$ complex.[12–18] Here, [10]CPP, featuring a cavity with a diameter of 13.9 Å,[19] encloses C_{60}, which has a diameter of 7 Å.[20] This leads to an intermolecular C–C distance of roughly 0.35 nm, which strongly resembles the interlayer spacing of graphite (0.34 nm)[21] and is hence considered the ideal size difference. [11]CPP and [12]CPP exhibit larger diameters of ≈15 (ref. 22) and ≈16.5 Å.[23] Accordingly, these CPPs are expected to preferably encapsulate fullerene guests larger than C_{60}. For example,

[a]Department of Chemistry and Pharmacy, Friedrich-Alexander-Universität Erlangen Nürnberg, 91058 Erlangen, Germany. E-mail: thomas.drewello@fau.de
[b]Institute of Computational Chemistry and Catalysis and Department of Chemistry, University of Girona, 17003 Girona, Catalonia, Spain. E-mail: miquel.sola@udg.edu
[c]Department of Chemistry, University of Texas at El Paso, El Paso, Texas 79968, USA
[d]Institut Català d'Investigació Química, 43007 Tarragona, Catalonia, Spain
†Electronic supplementary information (ESI) available. See DOI: https://doi.org/10.1039/d4nr02287d
‡These authors contributed equally to this work and share first authorship.

C_{70} adopts lying, standing, and half-lying orientations when encapsulated by [10]CPP, [11]CPP, and [12]CPP, respectively.[24] There are also reports suggesting complex formation between [11]CPP and C_{76} or C_{78},[22] while [12]CPP was identified as a suitable host for C_{84}.[14]

Several studies focused on the CPP-fullerene complexes given their uses in fullerene purification and selective functionalization,[16,25] fullerene radical stabilization[26,27] with interest in energy storage and conversion applications such as quantum information and solar cell technology,[28] construction of rotaxanes[29,30] and interlocked structures, controlled release, *etc.*[31] However, the number of reports covering the complex formation of CPPs with EMFs is very limited.[22,32–37] Itami *et al.* demonstrated that $Gd@C_{82}$ is selectively bound by [11]CPP in a mixture with various empty fullerenes.[33] In addition, we and other researchers have recently reported an enhanced stability of the $[10]CPP \supset Li^+@C_{60}$ host–guest system compared to $[10]CPP \supset C_{60}$.[38–41] Interestingly, the computational investigation of [11]CPP complexes with mono- and dimetallic EMFs revealed no significant dependence of the complex stability on the nature of the endohedral species.[22] Thus, it remains unclear whether the electronic nature of endohedral clusters and the corresponding charge transfer to the fullerene cage contributes to a stronger binding with CPPs in comparison to complexes with pristine fullerenes of similar size. On the other hand, the size selectivity of [11] and [12]CPP towards larger fullerene cores remains also unclear. Several studies suggest that [11]CPP is the ideal host for fullerenes with a $C_{80/82}$ skeleton,[22,32,33] while others works show that [12]CPP forms very stable complexes with C_{78}–C_{84} based fullerenes.[34,35,37,42]

This investigation compares host–guest complexes of [10–12]CPP with the pristine fullerenes $C_{76/78/84}$ and the EMFs $Sc_3N@D_{3h}$-C_{78}, $Sc_3N@D_{5h}$-C_{80}, and $M_3N@I_h$-C_{80} (M = Sc, Y, Lu, Gd) aiming at the establishment of trends in their stability. Electrospray ionization (ESI) mass spectrometry (MS) in combination with energy-resolved tandem mass spectrometry has proven to be a very suitable tool for the analysis of CPPs and their non-covalent complexes with C_{60} and C_{70}.[15,43] This technique is used in combination with density functional theory (DFT) calculations of ionization potentials (IPs) and fragmentation energies to contribute to a deeper understanding of the obtained experimental results.

Results and discussion

The first set of experiments is concerned with the complexation of [10–12]CPP with the pristine fullerenes $C_{76,78,84}$ using ESI MS. While of interest in its own right, this study also aims at the determination of the ideal CPP host size for the desired formation of complexes with C_{78}- and C_{80}-based EMFs. Thus the pristine fullerenes $C_{76,78,84}$ cover those fullerene sizes employed in the EMFs, in particular as empty C_{80} was not available to us. Complexation with the three fullerenes leads to very similar results. While the mass spectra of the pristine fullerenes $C_{76/78}$ can be found in the ESI (Fig. S1 and S2†), C_{84} is taken as a representative and discussed here in more detail. The C_{84} sample used in this experiment contained a mixture of the two most abundant isomers D_2 and D_{2d}. Previous work on the complexation of C_{84} with [10] and [12]CPP demonstrated that in both cases the D_2 isomer forms the most stable complexes.[14] So far, complexation between [11]CPP and C_{84} has not yet been studied.

Fig. 1 depicts the positive-ion mode mass spectra of solutions containing either [10], [11], or [12]CPP and C_{84}. In all spectra, the CPP radical cation represents the most abundant
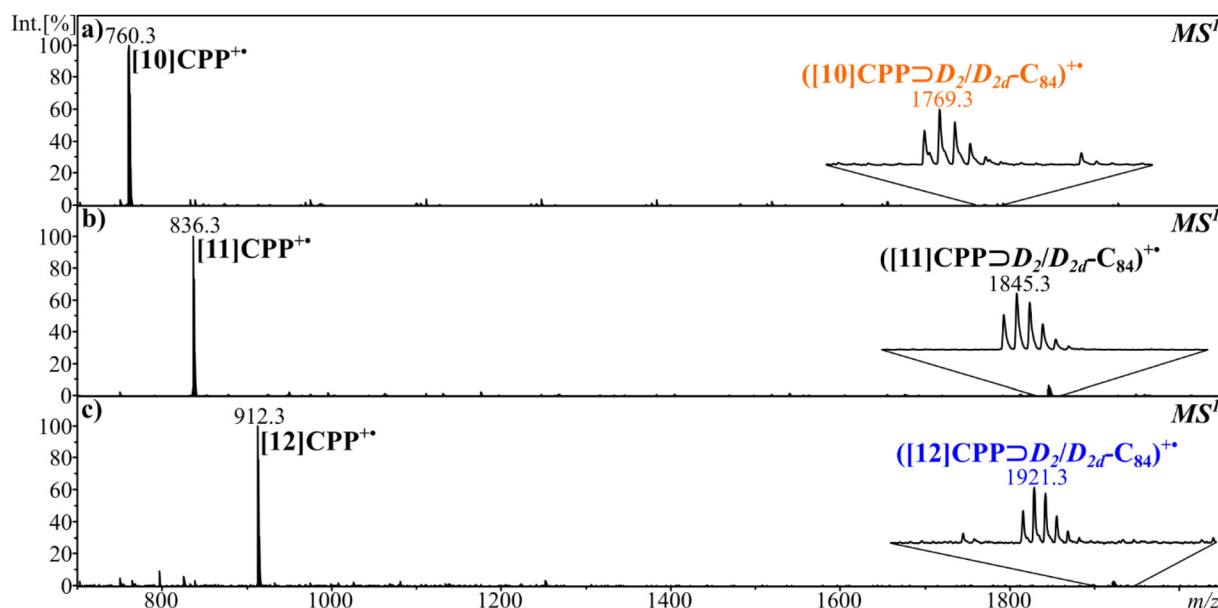

Fig. 1 Positive-ion mode ESI MS^1 spectra of solutions containing C_{84} and (a) [10]CPP, (b) [11]CPP or (c) [12]CPP.

species. Additionally, a signal corresponding to the respective host–guest complex is observed for all three mixtures, thereby demonstrating that all of the examined CPPs are able to form a host–guest complex with C_{84}. The $([11]CPP \supset C_{84})^{+\bullet}$ complex is most abundantly formed, followed by $([12]CPP \supset C_{84})^{+\bullet}$ and $([10]CPP \supset C_{84})^{+\bullet}$.

To identify the most stable host–guest complex among $([10–12]CPP \supset C_{76/78/84})^{+\bullet}$, we performed energy-resolved collision-induced dissociation experiments (ER-CID). For this type of experiment, the ion of interest is mass selected and subsequently submitted to multiple collisions with a stationary collision gas (N_2), whereby the collision energy is stepwise increased to eventually induce complete dissociation. The collision energy, E_{50}, at which 50% of the parent ions have dissociated into their daughter ions is chosen as a relative measure of stability.

Fig. 2c provides the breakdown graphs of $([10–12]CPP \supset C_{84})^{+\bullet}$. We found that [10]CPP forms the least stable complex followed by [12]CPP. This observation is in good

agreement with previous calculations[14] but the first experimental prove. [11]CPP forms the most stable inclusion complex with an E_{50} value of 0.203 V, confirming the best size match. According to our calculations, an average non-covalent C···C distance between [11]CPP and D_2-C_{84}/D_{2d}-C_{84} in the interacting area is 3.41/3.37 Å. Hence, the ideal size difference criterion is met. In the breakdown graphs of $([10–12]CPP \supset C_{76/78})^{+\bullet}$, [11]CPP is also the best host (Fig. 2a and b). Comparing the complexes with $C_{76/78/84}$, two trends become evident (Fig. S1, ESI†). First, complexes with [11]CPP and [12]CPP become more stable with increasing fullerene size which we relate to an increase in the number of interacting π-orbitals. Second, complexes with the [10]CPP host exhibit the opposite trend and $C_{76/78}$ complexes are more stable than the complex with C_{84}. This indicates that the latter is too large for the rather small [10]CPP host. In the following, we will only discuss complex formation between the EMFs and [11]CPP since it is the most suitable host. The measurements with [10] and [12]CPP can be found in the ESI, Fig. S2 and S3.†

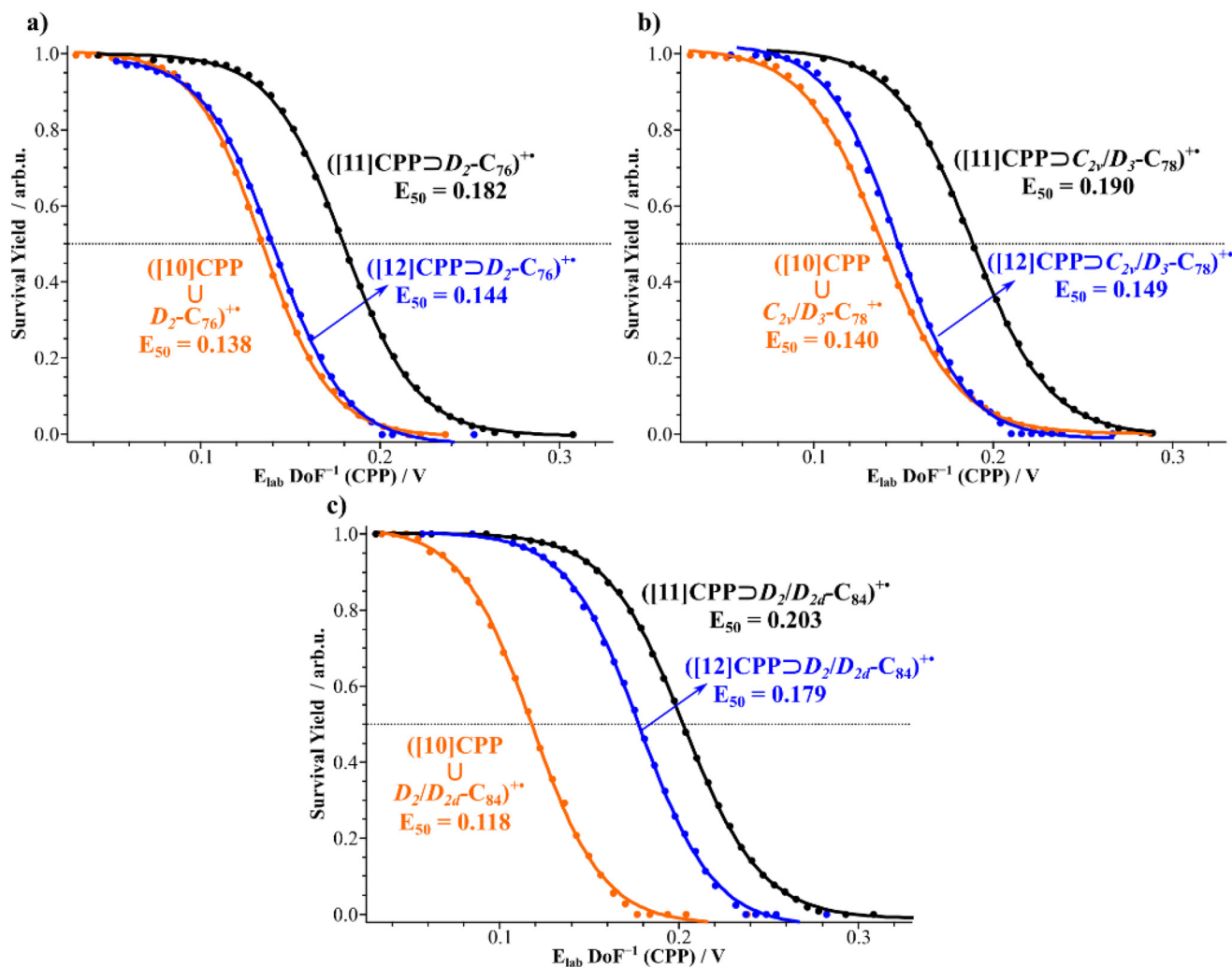**Fig. 2** Energy-resolved collision-induced dissociation graphs of (a) $([10–12]CPP \supset D_2\text{-}C_{76})^{+\bullet}$, (b) $([10–12]CPP \supset C_{2v}/D_3\text{-}C_{78})^{+\bullet}$ and (c) $([10–12]CPP \supset D_{2/2d}\text{-}C_{84})^{+\bullet}$.

Fig. 3a shows the MS^1 spectrum of a mixture of [11]CPP and $Y_3N@I_h$-C_{80}. Again, the most dominant signal in the spectrum is $[11]CPP^{+\bullet}$ at m/z 836. In contrast to pristine C_{84}, an additional signal corresponding to the radical cation of $Y_3N@C_{80}$ is observed at m/z 1240, indicating a reduced ionization potential of the endohedral fullerene. Besides these two species, the host–guest complex $([11]CPP \supset Y_3N@C_{80})^{+\bullet}$ can be identified at m/z 2078. The MS^1 spectra with C_{80} encapsulating other metal clusters (M = Sc, Gd and Lu) exhibit analog signals and are shown in Fig. S4–S6.†

To gain insight into the charge distribution of the studied host–guest complexes, a MS^2 experiment was performed (Fig. 3b). Dissociation of $([11]CPP \supset Y_3N@C_{80})^{+\bullet}$ leads to the formation of radical cations of [11]CPP and $Y_3N@C_{80}$. Surprisingly and contrary to what was observed for empty fullerenes, the more abundant fragment ion is $(Y_3N@C_{80})^{+\bullet}$ even though the MS^1 spectrum was dominated by $[11]CPP^{+\bullet}$. Taking into account the MS^2 spectra of other $M_3N@C_{80}$ complexes as well as their calculated IPs (Fig. S7–S9 and Table S1†), a certain trend becomes evident. If the EMF exhibits a low IP, an intense fullerene signal is observed. On the other hand, when EMFs have large IPs, the intensity of the CPP signal increases (Fig. S10, ESI†).

Another factor that can have an impact on the charge distribution upon fragmentation is a partial charge transfer in [n]CPP $\supset$ EMF complexes. However, the results of Mulliken population analysis for the [11]CPP $\supset$ La@C_{82}[32] and [12]CPP $\supset Sc_2C_2@C_{2n}$[42] complexes suggest a very small amount of charge transfer between the host and guest molecules (0.07–0.08e). Thus, the intensities of the signals are primarily determined by the IPs of CPPs and EMFs.

Furthermore, the geometry of the carbon cage needs to be considered due to its influence on the electronic properties of the respective EMFs. For instance, C_{80} based EMFs exist in two isomeric forms: I_h and D_{5h}. In 2005, Echegoyen et al.[44] demonstrated that the oxidation potential of the less abundant D_{5h} isomer of $Sc_3N@C_{80}$ is 0.27 V less positive compared to the I_h isomer, thus it can be oxidized much more easily. Exploiting

this difference, they achieved separation of the two isomers with a suitable oxidation agent.[44,45] To evaluate the impact of the cage isomerism on the host–guest chemistry of the EMFs, we also compared the MS^2 spectra of complexes between [11]CPP and the two isomers of $Sc_3N@C_{80}$ (Fig. 4a and b). Indeed, the spectra reveal a significant difference regarding the charge distribution upon dissociation. In the case of the D_{5h} isomer, almost no charge is located at the CPP, and the daughter ion spectrum is dominated by the $Sc_3N@C_{80}^{+\bullet}$ signal. Contrarily, the MS^2 spectrum of the complex between [11]CPP and the I_h isomer yields 24% of $[11]CPP^{+\bullet}$. Considering that both complexes differ only by the geometry of the carbon cage, it is interesting to note that collision-induced dissociation provides such a clear distinction between the two fullerene isomers.

Next, we turned our attention to $Sc_3N@D_{3h}$-C_{78}, which has a carbon cage of different size and symmetry. $Sc_3N@C_{78}$ is a specific EMF with a non-negligible mixing of the molecular orbitals of the cluster and the fullerene cage.[46,47] Fig. 4c illustrates the MS^2 spectrum of the $([11]CPP \supset Sc_3N@D_{3h}$-$C_{78})^{+\bullet}$ complex ion, which is very similar to the spectrum of $([11]CPP \supset Sc_3N@D_{5h}$-$C_{80})^{+\bullet}$. This is in complete agreement with the value of the oxidation potential, which is much lower for $Sc_3N@D_{3h}$-C_{78} than for $Sc_3N@I_h$-C_{80}, but closer to the $Sc_3N@D_{5h}$-C_{80} isomer.[45,48] Here, the [11]CPP radical cation is not detected, and only $Sc_3N@C_{78}^{+\bullet}$ is formed. Hence, our experiments show that the encapsulated nitride metal cluster, the cage symmetry as well as the cage size influence the electronic properties and fragmentation pathway of the complexes with CPPs.

We performed ER-CID experiments with all successfully formed fullerene/EMF based host–guest complexes. Fig. 5a shows a comparison of the breakdown curves of [11]CPP based [1 : 1] complexes with D_2-C_{76}, C_{2v}/D_3-C_{78}, D_2/D_{2d}-C_{84}, $Sc_3N@D_{3h}$-C_{78} and $M_3N@I_h$-C_{80} (M = Sc, Y, Lu, Gd) as guests. Similar curves for [10]- and [12]CPP based complexes are shown in Fig. S11, ESI.† It is observed that the EMFs form significantly more stable complexes than the pristine fullerenes, which is consistent with previous experimental studies.[33,38–40]
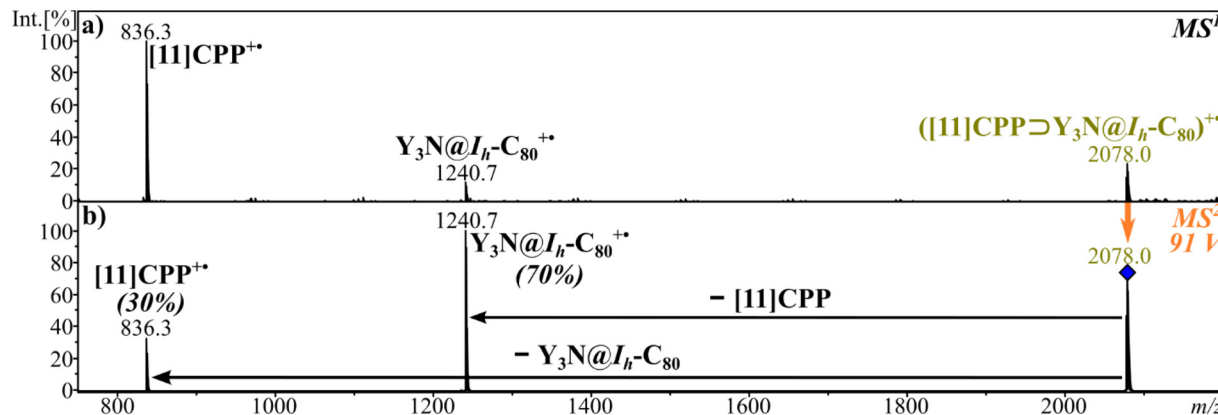

Fig. 3 (a) Positive-ion mode ESI MS^1 spectrum of a solution containing [11]CPP and $Y_3N@I_h$-C_{80}, (b) MS^2 spectrum of the complex $([11]CPP \supset Y_3N@I_h$-$C_{80})^{+\bullet}$.
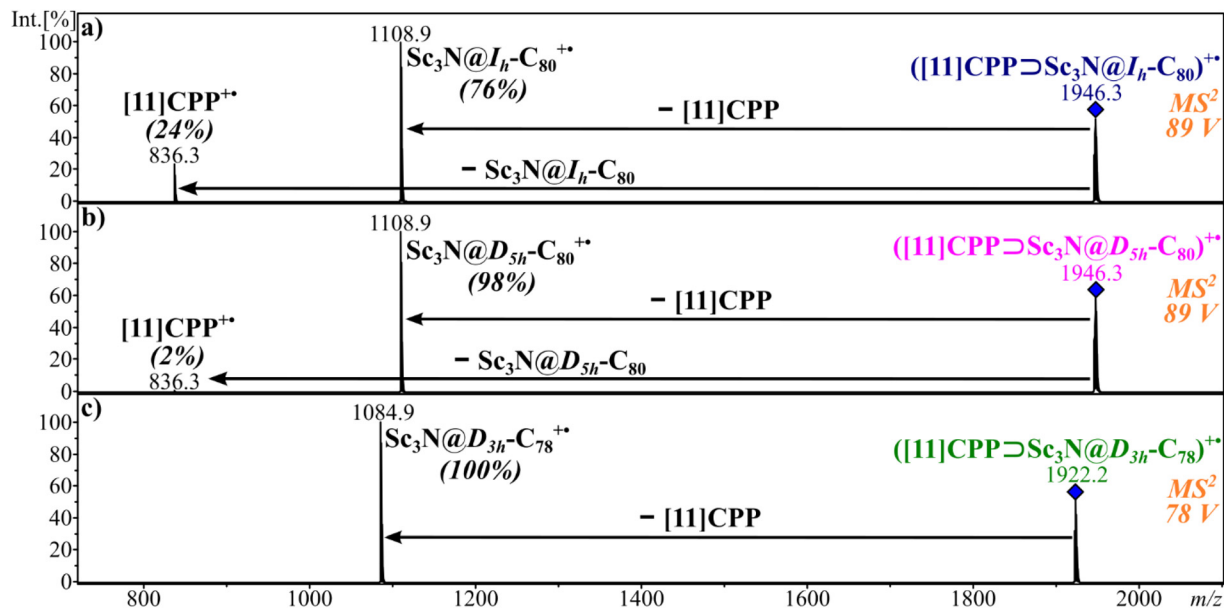
Fig. 4 MS^2 spectra of (a) ([11]CPP ⊃ Sc$_3$N@I_h-C$_{80}$)$^{+•}$, (b) ([11]CPP ⊃ Sc$_3$N@D_{5h}-C$_{80}$)$^{+•}$ and (c) ([11]CPP ⊃ Sc$_3$N@D_{3h}-C$_{78}$)$^{+•}$.
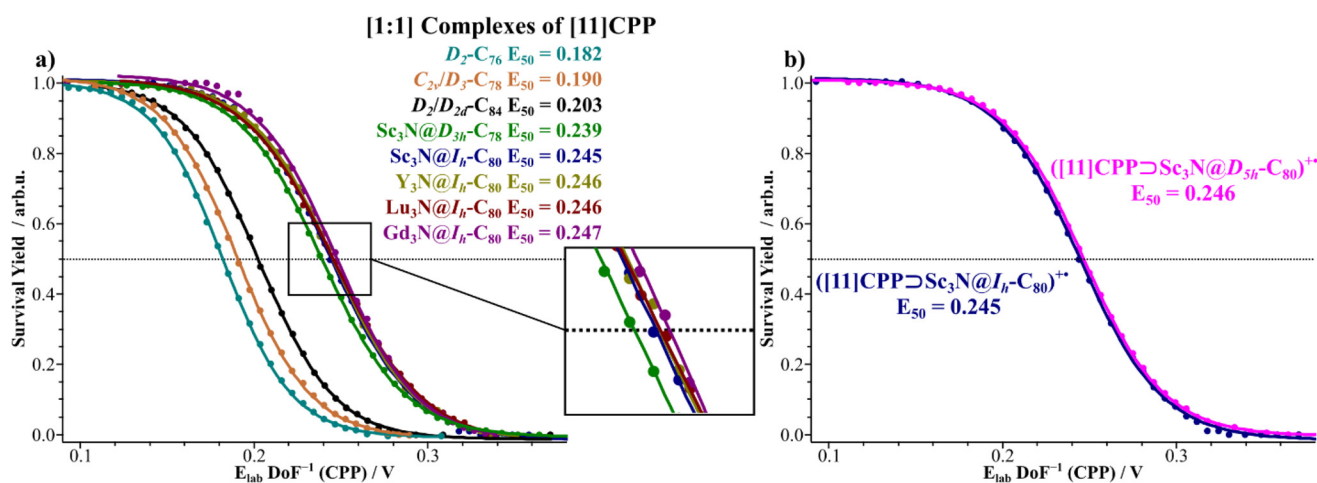
Fig. 5 Energy-resolved collision-induced dissociation graphs of host–guest complexes between [11]CPP and (a) D_2-C$_{76}$, C_{2v}/D_3-C$_{78}$, D_2/D_{2d}-C$_{84}$, Sc$_3$N@D_{3h}-C$_{78}$ and M$_3$N@I_h-C$_{80}$ (M = Sc, Y, Gd, Lu); (b) Sc$_3$N@I_h-C$_{80}$ and Sc$_3$N@D_{5h}-C$_{80}$.

The stability of such complexes can possibly be explained not only by the shape and size complementarity but also by the electrostatic complementarity of CPPs and EMFs, which was confirmed by positive and negative regions of the molecular electrostatic potential (MEP).[22] In the case of the metal nitride cluster fullerenes, the carbon cage above and below the metal cluster is negatively charged, while the area around the cluster has positive potential (Fig. S12, ESI†). The positive potential around the Sc$_3$N cluster is slightly higher than around the Y$_3$N and Lu$_3$N clusters. On the other hand, the cavity of CPP has negative MEP regions, thus preferring to encapsulate electron-deficient species.[22,41] Consequently, the metal nitride cluster inside EMFs is oriented in the plane of [11]CPP, thereby providing electrostatic complementarity.

The EMF based complexes with CPPs reveal three clear trends. First, the stability of complexes with [n]CPPs decreases in the following order: [11]CPP > [12]CPP > [10]CPP, which is clearly visible in Fig. 6. Second, the slightly smaller C$_{78}$ core leads to an observable decrease in stability which we attribute to less stabilization *via* π–π interactions. This observation is also consistent with the complexes of pristine fullerenes (Fig. 2 and 5a). Third, all complexes of EMFs with the C$_{80}$ skeleton show similar stability despite the different metal clusters encapsulated. This indicates that for the investigated M$_3$N clusters the nature of the encapsulated metal cluster does not affect the interaction strength. We emphasize that these findings are obtained for the cationic complexes and that the behavior of the corresponding neutral complexes might deviate.
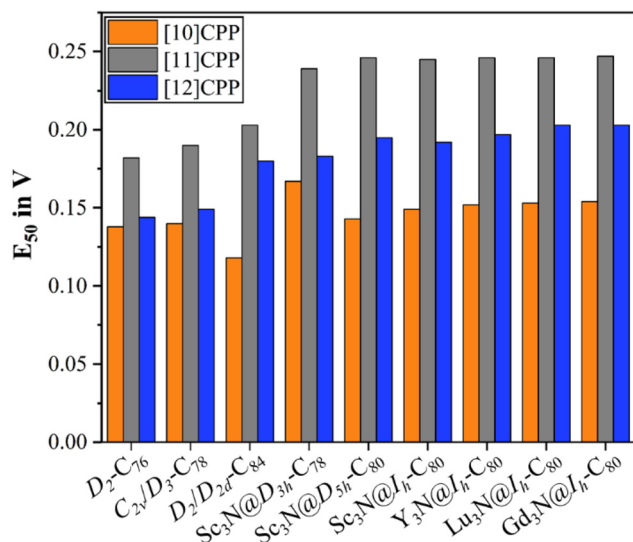
Fig. 6 Comparison of the E_{50} values (collision energy) for the studied host–guest complexes between [n]CPP (n = 10, 11, 12) and various fullerenes.

Fig. 5b shows a direct comparison of the ([11]CPP ⊃ Sc$_3$N@C$_{80}$)$^{+\bullet}$ complexes for I_h and D_{5h} isomers of C$_{80}$. Although a clear difference between the two isomers was observed in the MS^2 spectra (Fig. 4), the analysis of the breakdown curves reveals that both complexes are isoenergetic. Thus, we assume that the stability of the complex does not significantly depend on the cage isomer if the attractive van der Waals interactions are not altered. This observation was further confirmed by the similar NCI (non-covalent interaction) isosurfaces[49] of the [11]CPP ⊃ I_h-Sc$_3$N@C$_{80}$ and [11]CPP ⊃ D_{5h}-Sc$_3$N@C$_{80}$ complexes (Fig. S13†).

Computational studies

Non-covalent interactions play an important role in the supramolecular chemistry of carbon nanostructures. The accurate description of such interactions is a primary goal in the study of fullerene-CPP complexes. However, this task presents a challenge for computational methods due to the significant contribution of dispersion interactions. Density functional theory (DFT) offers a good balance between computational cost and accuracy.[50,51] In particular, a range-separated hybrid ωB97M-V density functional with VV10 nonlocal correlation provides fairly accurate results for intermolecular interaction energies.[52–54]

The geometry of the complexes in the neutral and radical cation forms was optimized using the DFT BLYP functional[55,56] with D3(BJ) dispersion correction[57,58] and def2-SVP basis set.[59,60] The M$_3$N (M = Sc, Y, Lu) clusters prefer a flat geometry within the fullerene I_h-C$_{80}$ and are able to freely rotate inside the cage, which is consistent with the experimental and previous computational results.[61–63] However, the large Gd$_3$N cluster cannot maintain a flat geometry and is

forced into a pyramidal shape inside the cage.[64] In complexes with [11]CPP, the M$_3$N@C$_{80}$ fullerenes are located at the center of the host molecule in such a way that the metal cluster lies in the plane of [11]CPP. This arrangement allows for the best distribution of attractive (electrostatic, dispersion) and repulsive forces.[22]

To evaluate the effect of the metal cluster on the stability of the host–guest complexes, we compared the [11]CPP ⊃ M$_3$N@C$_{80}$ complexes with the complex formed by the C$_{84}$ fullerene, since the diameter of its stable isomer is less than 5% larger than the diameter of the M$_3$N@C$_{80}$ fullerenes. The commercial C$_{84}$ fullerene is a mixture of the D_{2d} and D_2 structural isomers, thus we considered the complexes with [11]CPP for each of them. The most energetically stable isomer is the nearly spherical D_{2d} isomer, while the D_2 isomer is very similar to D_{2d} in both energy and shape.[65] Their host–guest complexes are also isoenergetic, with an energy difference of less than 1 kcal mol^{-1} at the BLYP-D3(BJ)/def2-SVP level. An average distance for non-covalent C⋯C contacts is 3.37 and 3.41 Å for the D_{2d} and D_2 isomer, respectively.

To understand the differences in the experimental MS^1 and MS^2 spectra, we computationally studied the electronic properties of the host–guest complexes and their separated units at the ωB97M-V/def2-TZVPP//BLYP-D3(BJ)/def2-SVP level. In the MS^1 spectra, the M$_3$N@C$_{80}^{+\bullet}$ radical cation could be observed while no C$_{84}^{+\bullet}$ signals appeared. This observation is associated with the lower ionization potential (IP) of the studied EMFs compared to the pristine C$_{84}$. The ion formation proceeds in our experiments through electrochemical oxidation within the ESI source and the calculated IP is used here as a measure to indicate the ease of electron loss from the neutral molecular entity. The IP was calculated as the energy difference between the neutral and cationic forms of the system at the optimized geometry of the neutral species. According to the results, IPs of M$_3$N@I_h-C$_{80}$ (M = Sc, Y, Lu) EMFs are 0.4–0.5 eV lower than that of C$_{84}$. Notably, the IPs of the EMFs are comparable with the IP of [11]CPP (Table S1†). Therefore, both EMF and CPP signals were detected in the MS^1 spectra. The IP also influences the signal intensity. For example, the larger signal intensity of Sc$_3$N@I_h-C$_{80}^{+\bullet}$ compared to [11]CPP$^{+\bullet}$ agrees with a difference in their IPs (0.07 eV higher for [11]CPP). We obtained the following trend regarding the IP values: IP (Sc$_3$N@D_{5h}-C$_{80}$) < IP (Sc$_3$N@I_h-C$_{80}$) < IP ([11]CPP) ≈ IP (Lu$_3$N@I_h-C$_{80}$) ≈ IP (Y$_3$N@I_h-C$_{80}$) < IP (C$_{84}$). This trend is consistent with the experimentally determined trend regarding the oxidation potentials of the EMFs,[66,67] see Fig. S14 in ESI.† The IP of empty I_h-C$_{80}$ is even lower than the IPs of EMFs, as this isomer has a 4-fold degenerate HOMO occupied by only two electrons, making it unstable. However, it is stabilized by the endohedral cluster, as its HOMO is filled by six extra electrons from the cluster, resulting in a stable closed-shell electronic structure.

In addition, the MS^1 signals of the [11]CPP ⊃ M$_3$N@C$_{80}$ complexes were found to be more intense than the ones of the [11]CPP ⊃ C$_{84}$ complexes (Fig. 1, 3 and S4†), which is due to the [11]CPP ⊃ M$_3$N@C$_{80}$ complexes requiring less energy for

ionization. This is caused by a different electron density distribution over the frontier orbitals (Fig. S15†). When [11]CPP interacts with $M_3N@I_h$-C_{80}, its HOMO is stabilized by the positive electrostatic potential of EMF. As a result, the highest occupied molecular orbital (HOMO) of EMF-based host–guest complexes is mainly located not on [11]CPP but on the fullerene cage with an energy between −7.11 and −7.15 eV. In turn, the HOMO of [11]CPP ⊃ C_{84} is completely located on [11]CPP and lies much lower in energy than the HOMO of [11]CPP ⊃ $M_3N@I_h$-C_{80} (Table S2†). During the MS^1 experiment an electron is removed from the HOMO of the complexes, which is facilitated for the complexes of EMFs due to their higher-lying HOMO. After the loss of an electron, the electron density in $([n]CPP ⊃ M_3N@I_h$-$C_{80})^{+•}$ and $([n]CPP ⊃ C_{76,78,84})^{+•}$ is redistributed and all complexes have a similar electronic structure, with the spin density located on the fullerene cage (Table S3†).

The stability of the oxidized complexes was estimated referring to the energy required to break the radical cations of the studied complexes into two fragments. Table 1 shows the calculated energy values for two possible fragmentation pathways: (1) $[11]CPP^{+•} + M_3N@C_{80}$ and (2) $[11]CPP + M_3N@C_{80}^{+•}$ (Fig. 7). The results for the complexes with [10]CPP and [12]CPP are collected in Tables S4 and S5.† It can be seen that the fragmentation following pathway 1 is preferable for all complexes except for $([11]CPP ⊃ Sc_3N@I_h$-$C_{80})^{+•}$, where the two pathways are almost isoenergetic. The preference of the [11]CPP$^{+•}$ formation can be explained by comparing the ionization potentials of $M_3N@I_h$-C_{80} and [11]CPP fragments in the

complex (Table S3†). In all cases except $([11]CPP ⊃ Sc_3N@I_h$-$C_{80})^{+•}$, the IP of the [11]CPP fragment is lower than the IP of the EMF fragment, thus the probability of [11]CPP$^{+•}$ formation is slightly higher. For pathway 1, the fragmentation energies for the C_{84}-based complexes (≈59 kcal mol^{-1}) are lower than the energies for EMF-based complexes (≈64–67 kcal mol^{-1}). These results confirm the experimental finding that the EMFs form more stable complexes with [11]CPP than the pristine C_{84}. The histograms for computational and experimental results are presented in Fig. S16, ESI.† It is worth noting that comparing the BSSE-corrected binding energies for neutral [11]CPP complexes with pristine fullerenes and EMFs (Table S6†) leads to the same conclusion, but the differences between pristine fullerenes and EMFs are less pronounced than when comparing fragmentation energies.

The CPP-to-fullerene signal ratio observed in the MS^2 experiment is explained comparing the ΔE_{frag} values for the two fragmentation pathways. If the fragmentation energy for pathway 1 is much lower than for pathway 2, we observe only the [11]CPP$^{+•}$ signal in the MS^2 spectrum, as for the $([11]CPP ⊃ C_{84})^{+•}$ ion. On the other hand, if the fragmentation of the complex ion preferably follows pathway 2, we observe only the fullerene signal, as for $([11]CPP ⊃ Sc_3N@D_{3h}$-$C_{78})^{+•}$. In turn, if the fragmentation energies for both pathways are comparable, both [11]CPP$^{+•}$ and $M_3N@C_{80}^{+•}$ signals can be observed in the spectrum, as for the $([11]CPP ⊃ M_3N@C_{80})^{+•}$ ions.

The complexes with the Sc_3N cluster represent a special case with a prevalence of the fragmentation pathway 2

Table 1 Energies (ΔE_{frag}, in kcal mol^{-1}) for fragmentation of [11]CPP ⊃ fullerene ions along different pathways calculated at the ωB97M-V/def2-TZVPP//BLYP-D3(BJ)/def2-SVP level and experimental ratio of signals

Complex	ΔE_{frag} (pathway 1)	ΔE_{frag} (pathway 2)	Difference[a]	CPP-to-fullerene ratio[b]
$([11]CPP ⊃ Sc_3N@I_h$-$C_{80})^{+•}$	67.93	67.60	−0.33	24 : 76
$([11]CPP ⊃ Y_3N@I_h$-$C_{80})^{+•}$	63.77	69.17	5.40	30 : 70
$([11]CPP ⊃ Lu_3N@I_h$-$C_{80})^{+•}$	66.93	72.07	5.14	52 : 48
$([11]CPP ⊃ Gd_3N@I_h$-$C_{80})^{+•}$	63.58	70.26	6.68	51 : 49
$([11]CPP ⊃ D_{2d}$-$C_{84})^{+•}$	58.64	72.43	13.79	100 : 0
$([11]CPP ⊃ D_2$-$C_{84})^{+•}$	58.95	71.29	12.34	100 : 0

[a] Difference = ΔE_{frag}(pathway 2) − ΔE_{frag}(pathway 1). [b] [11]CPP vs. fullerene ratio of the intensities observed in experimental MS^2 spectra.

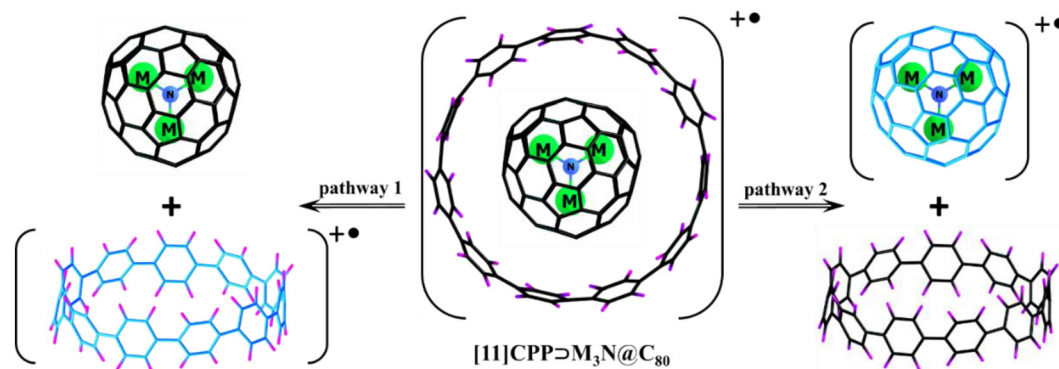**Fig. 7** Two possible fragmentation pathways for $([11]CPP ⊃ M_3N@C_{80})^{+•}$ (M = Sc, Y, Lu, Gd) in the ER-CID experiment.

(Table S7†). Accordingly, the fullerene signal dominates in the corresponding MS^2 spectra. The IPs of $Sc_3N@D_{5h}-C_{80}$ and $Sc_3N@D_{3h}-C_{78}$ are 6.61 and 6.54 eV at the ωB97M-V/TZVPP level, respectively, being significantly lower than the IPs of $Sc_3N@I_h-C_{80}$ (7.00 eV) and [11]CPP (7.07 eV). Thus, the formation of their radical cations upon dissociation is more favorable than the formation of [11]CPP$^{+•}$. The correlation between the calculated preferred fragmentation pathway and intensity of the fullerene signal can be found in Fig. S17, ESI.†

Conclusion

We have successfully investigated host–guest complexes between [10–12]CPP and D_2-C_{76}, C_{2v}/D_3-C_{78}, $D_2/D_{2d}-C_{84}$, $Sc_3N@D_{3h}-C_{78}$, $Sc_3N@D_{5h}-C_{80}$, and $M_3N@I_h-C_{80}$ (M = Sc, Y, Lu, Gd) by means of tandem mass spectrometry and DFT calculations. The soft ESI technique enabled the successful ionization and transfer of [1 : 1] complexes of all investigated systems from solution into the gas-phase. Using ER-CID experiments, we observed that [11]CPP is the best host for fullerenes with a $C_{76/78/80/84}$ skeleton. It also became evident that [n]CPPs form more stable complexes with EMFs than with pristine fullerenes of similar size. The computational results fully confirm the experimental findings and explain the prevalence of EMF or CPP signals in the spectra by the trend in ionization potentials. Moreover, the difference in the fragmentation energy for two possible pathways, (1) [11]CPP$^{+•}$ + $M_3N@C_{80}$ and (2) [11]CPP + $M_3N@C_{80}^{+•}$, correlates with the experimentally observed CPP-to-fullerene signal ratio. The results suggest that an energy difference greater than 10 kcal mol^{-1} results in the detection of only one signal in the MS^2 spectrum. Otherwise, both [n]CPP$^{+•}$ and $M_3N@C_{80}^{+•}$ signals are observed. The present study provides essential molecular-level insights into the key factors of the complexation between [n]CPPs and pristine/endohedral fullerenes.

Data availability

The data supporting this article have been included as part of the ESI,† which contains detailed description of the experiment and DFT calculations, additional mass spectra and computational results, as well as Cartesian coordinates of the complexes. Additional data are available at Zenodo https://doi.org/10.5281/zenodo.13254671.

Conflicts of interest

There are no conflicts to declare.

Acknowledgements

References

1 S. Iijima, *Nature*, 1991, **354**, 56–58.
2 B. W. Smith, M. Monthioux and D. E. Luzzi, *Nature*, 1998, **396**, 323–324.
3 K. Hirahara, K. Suenaga, S. Bandow, H. Kato, T. Okazaki, H. Shinohara and S. Iijima, *Phys. Rev. Lett.*, 2000, **85**, 5384–5387.
4 B. W. Smith, D. E. Luzzi and Y. Achiba, *Chem. Phys. Lett.*, 2000, **331**, 137–142.
5 A. Débarre, R. Jaffiol, C. Julien, D. Nutarelli, A. Richard and P. Tchénio, *Phys. Rev. Lett.*, 2003, **91**, 085501.
6 P. W. Chiu, G. Gu, G. T. Kim, G. Philipp, S. Roth, S. F. Yang and S. Yang, *Appl. Phys. Lett.*, 2001, **79**, 3845–3847.
7 A. N. Khlobystov, K. Porfyrakis, D. A. Britz, M. Kanai, R. Scipioni, S. G. Lyapin, J. G. Wiltshire, A. Ardavan, D. Nguyen-Manh, R. J. Nicholas, D. G. Pettifor, T. J. S. Dennis and G. A. D. Briggs, *Mater. Sci. Technol.*, 2004, **20**, 969–974.
8 Y. Xu and M. von Delius, *Angew. Chem., Int. Ed.*, 2020, **59**, 559–573.
9 R. Jasti, J. Bhattacharjee, J. B. Neaton and C. R. Bertozzi, *J. Am. Chem. Soc.*, 2008, **130**, 17646–17647.
10 D. Lu, Q. Huang, S. Wang, J. Wang, P. Huang and P. Du, *Front. Chem.*, 2019, **7**, 668.
11 J. M. Lehn, *Angew. Chem., Int. Ed. Engl.*, 1988, **27**, 89–112.
12 T. Iwamoto, Y. Watanabe, T. Sadahiro, T. Haino and S. Yamago, *Angew. Chem., Int. Ed.*, 2011, **50**, 8342–8344.
13 J. Xia, J. W. Bacon and R. Jasti, *Chem. Sci.*, 2012, **3**, 3018–3021.
14 M. B. Minameyer, Y. Xu, S. Frühwald, A. Görling, M. von Delius and T. Drewello, *Chem. – Eur. J.*, 2020, **26**, 8729–8741.
15 M. Freiberger, M. B. Minameyer, I. Solymosi, S. Frühwald, M. Krug, Y. Xu, A. Hirsch, T. Clark, D. Guldi, M. von Delius, K. Amsharov, A. Görling, M. E. Pérez-Ojeda and T. Drewello, *Chem. – Eur. J.*, 2023, **15**, 5665–5670.
16 E. Ubasart, O. Borodin, C. Fuertes-Espinosa, Y. Xu, C. García-Simón, L. Gómez, J. Juanhuix, F. Gándara, I. Imaz, D. Maspoch, M. von Delius and X. Ribas, *Nat. Chem.*, 2021, **13**, 420–427.
17 J. Volkmann, D. Kohrs and H. A. Wegner, *Chem. – Eur. J.*, 2023, e202300268.
18 G. Pareras, S. Simon, A. Poater and M. Solà, *J. Org. Chem.*, 2022, **87**, 5149–5157.

19 E. Kayahara, Y. Sakamoto, T. Suzuki and S. Yamago, *Org. Lett.*, 2012, **14**, 3284–3287.

20 W. I. F. David, R. M. Ibberson, J. C. Matthewman, K. Prassides, T. J. S. Dennis, J. P. Hare, H. W. Kroto, R. Taylor and D. R. M. Walton, *Nature*, 1991, **353**, 147–149.

21 P. Delhaes, *Graphite and Precursors*, CRC Press, 2001.

22 I. González-Veloso, E. M. Cabaleiro-Lago and J. Rodríguez-Otero, *Phys. Chem. Chem. Phys.*, 2018, **20**, 11347–11358.

23 Y. Segawa, S. Miyamoto, H. Omachi, S. Matsuura, P. Šenel, T. Sasamori, N. Tokitoh and K. Itami, *Angew. Chem., Int. Ed.*, 2011, **50**, 3244–3248.

24 K. Yuan, Y.-J. Guo and X. Zhao, *J. Phys. Chem. C*, 2015, **119**, 5168–5179.

25 Y. Xu, R. Kaur, B. Wang, M. B. Minameyer, S. Gsänger, B. Meyer, T. Drewello, D. M. Guldi and M. von Delius, *J. Am. Chem. Soc.*, 2018, **140**, 13413–13420.

26 A. Stergiou, J. Rio, J. H. Griwatz, D. Arčon, H. A. Wegner, C. P. Ewels and N. Tagmatarchis, *Angew. Chem., Int. Ed.*, 2019, **58**, 17745–17750.

27 Y. Tanuma, A. Stergiou, A. B. Bobnar, M. Gaboardi, J. Rio, J. Volkmann, H. A. Wegner, N. Tagmatarchis, C. P. Ewels and D. Arčon, *Nanoscale*, 2021, **13**, 19946–19955.

28 Y. Tang, J. Li, P. Du, H. Zhang, C. Zheng, H. Lin, X. Du and S. Tao, *Org. Electron.*, 2020, **83**, 105747.

29 Y. Xu, B. Wang, R. Kaur, M. B. Minameyer, M. Bothe, T. Drewello, D. M. Guldi and M. von Delius, *Angew. Chem., Int. Ed.*, 2018, **57**, 11549–11553.

30 I. Solymosi, J. Sabin, H. Maid, L. Friedrich, E. Nuin, M. E. Perez-Ojeda and A. Hirsch, *Org. Mater.*, 2022, **4**, 73–85.

31 X. Chang, Y. Xu and M. von Delius, *Chem. Soc. Rev.*, 2024, **53**, 47–83.

32 T. Iwamoto, Z. Slanina, N. Mizorogi, J. Guo, T. Akasaka, S. Nagase, H. Takaya, N. Yasuda, T. Kato and S. Yamago, *Chem. – Eur. J.*, 2014, **20**, 14403–14409.

33 Y. Nakanishi, H. Omachi, S. Matsuura, Y. Miyata, R. Kitaura, Y. Segawa, K. Itami and H. Shinohara, *Angew. Chem., Int. Ed.*, 2014, **53**, 3102–3106.

34 C. Zhao, H. Meng, M. Nie, X. Wang, Z. Cai, T. Chen, D. Wang, C. Wang and T. Wang, *J. Phys. Chem. C*, 2019, **123**, 12514–12520.

35 J. Zhang, C. Zhao, H. Meng, M. Nie, Q. Li, J. Xiang, Z. Zhang, C. Wang and T. Wang, *Carbon*, 2020, **161**, 694–701.

36 J. Zhang, L. Qiu, L. Liu, Y. Liu, P. Cui, F. Wang and Z. Zhang, *Nanomaterials*, 2022, **12**, 1408.

37 J. Liang, Y. Lu, J. Zhang, L. Qiu, W. Li, Z. Zhang, C. Wang and T. Wang, *Dalton Trans.*, 2022, **51**, 10227–10233.

38 A. J. Stasyuk, O. A. Stasyuk, M. Solà and A. A. Voityuk, *Chem. Commun.*, 2019, **55**, 11195–11198.

39 H. Ueno, T. Nishihara, Y. Segawa and K. Itami, *Angew. Chem., Int. Ed.*, 2015, **54**, 3707–3711.

40 M. Freiberger, I. Solymosi, E. M. Freiberger, A. Hirsch, M. E. Pérez-Ojeda and T. Drewello, *Nanoscale*, 2023, **15**, 5665–5670.

41 I. González-Veloso, J. Rodríguez-Otero and E. M. Cabaleiro-Lago, *Phys. Chem. Chem. Phys.*, 2016, **18**, 31670–31679.

42 Y. Liu, W. Li, P. Li, Y. Guo, P. Cui and Z. Zhang, *RSC Adv.*, 2023, **13**, 4553–4563.

43 F. Schwer, S. Zank, M. Freiberger, R. Kaur, S. Frühwald, C. C. Robertson, A. Görling, T. Drewello, D. M. Guldi and M. von Delius, *Org. Mater.*, 2022, **4**, 7–17.

44 B. Elliott, L. Yu and L. Echegoyen, *J. Am. Chem. Soc.*, 2005, **127**, 10885–10888.

45 M. R. Cerón, F.-F. Li and L. Echegoyen, *Chem. – Eur. J.*, 2013, **19**, 7410–7415.

46 J. M. Campanera, C. Bo, M. M. Olmstead, A. L. Balch and J. M. Poblet, *J. Phys. Chem. A*, 2002, **106**, 12356–12364.

47 M. Krause, A. Popov and L. Dunsch, *ChemPhysChem*, 2006, **7**, 1734–1740.

48 L. Zhang, N. Chen, L. Fan, C. Wang and S. Yang, *J. Electroanal. Chem.*, 2007, **608**, 15–21.

49 E. R. Johnson, S. Keinan, P. Mori-Sánchez, J. Contreras-García, A. J. Cohen and W. Yang, *J. Am. Chem. Soc.*, 2010, **132**, 6498–6506.

50 R. Sedlak, T. Janowski, M. Pitoňák, J. Řezáč, P. Pulay and P. Hobza, *J. Chem. Theory Comput.*, 2013, **9**, 3364–3374.

51 R. Sure and S. Grimme, *J. Chem. Theory Comput.*, 2015, **11**, 3785–3801.

52 N. Mardirossian and M. Head-Gordon, *J. Chem. Phys.*, 2016, **144**, 214110.

53 A. Najibi and L. Goerigk, *J. Chem. Theory Comput.*, 2018, **14**, 5725–5738.

54 N. Mardirossian and M. Head-Gordon, *Mol. Phys.*, 2017, **115**, 2315–2372.

55 A. D. Becke, *Phys. Rev. A*, 1988, **38**, 3098–3100.

56 C. Lee, W. Yang and R. G. Parr, *Phys. Rev. B: Condens. Matter Mater. Phys.*, 1988, **37**, 785–789.

57 S. Grimme, J. Antony, S. Ehrlich and H. Krieg, *J. Chem. Phys.*, 2010, **132**, 154104.

58 S. Grimme, S. Ehrlich and L. Goerigk, *J. Comput. Chem.*, 2011, **32**, 1456–1465.

59 F. Weigend and R. Ahlrichs, *Phys. Chem. Chem. Phys.*, 2005, **7**, 3297–3305.

60 F. Weigend, *Phys. Chem. Chem. Phys.*, 2006, **8**, 1057–1065.

61 S. Stevenson, G. Rice, T. Glass, K. Harich, F. Cromer, M. R. Jordan, J. Craft, E. Hadju, R. Bible, M. M. Olmstead, K. Maitra, A. J. Fisher, A. L. Balch and H. C. Dorn, *Nature*, 1999, **401**, 55–57.

62 R. Valencia, A. Rodríguez-Fortea, A. Clotet, C. de Graaf, M. N. Chaur, L. Echegoyen and J. M. Poblet, *Chem. – Eur. J.*, 2009, **15**, 10997–11009.

63 M. Garcia-Borràs, S. Osuna, J. M. Luis, M. Swart and M. Solà, *Chem. – Eur. J.*, 2013, **19**, 14931–14940.

64 S. Osuna, R. Valencia, A. Rodríguez-Fortea, M. Swart, M. Solà and J. M. Poblet, *Chem. – Eur. J.*, 2012, **18**, 8944–8956.

65 Y. Ma, S. Y. Wang, J. Hu, Y. Zhou, X. N. Song and C. K. Wang, *J. Phys. Chem. A*, 2018, **122**, 1019–1026.

66 M. N. Chaur, F. Melin, A. L. Ortiz and L. Echegoyen, *Angew. Chem., Int. Ed.*, 2009, **48**, 7514–7538.

67 M. Zalibera, P. Rapta, A. A. Popov and L. Dunsch, *J. Phys. Chem. C*, 2009, **113**, 5141–5149.